OL | Organic Letters

pubs.acs.org/OrgLett Letter

Delocalization Effects and Tunable Emission in a Class of Charged Cyclazines with Nitrogen on the Periphery

Jais Kurian, Kanneth S. Shurooque, Venkatachalam Ramkumar, Lakshmi Chakkumkumarath,* and Muraleedharan Kannoth M.*

Cite This: *Org. Lett.* 2021, 23, 3354−3358 Read Online

ACCESS | Metrics & More | Article Recommendations | Supporting Information

ABSTRACT: A new class of cyclazine analogues with periphery reminiscent of an aza[10]annulene framework, tethered internally by an sp^3 carbon, is presented. In depth structure analysis based on NMR and X-ray diffraction data gave a deeper insight into the effect of electron delocalization on their structure and properties. A characteristic change in chemical shift positions suggested an aromatic ring current in these systems. Attractive emission properties in solid and solution states involving charge transfer is another highlight.

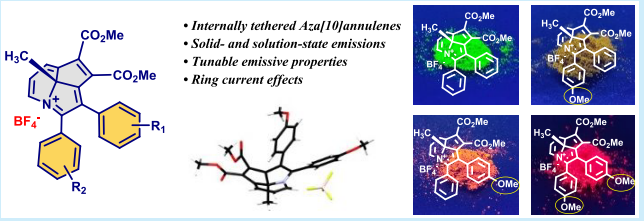

Downloaded via RUTGERS UNIV on May 15, 2021 at 07:46:20 (UTC).
See https://pubs.acs.org/sharingguidelines for options on how to legitimately share published articles.

"Aromaticity" is one of the most important fundamental concepts in chemistry that elegantly links electronic characteristics of molecules with a special type of bonding, reactivity, and properties.[1,2] Apart from delocalization solely through π-frameworks, involvement of σ bonds has also been demonstrated in systems like $PtZnH_5^-$.[3] In terms of chemical diversity, this area is enriched with numerous examples of neutral and charged cyclic polyenes,[4,5] expanded/macrocyclic porphyrins,[6−8] transition-metal clusters, etc.[9,10] Theoretical prediction of aromatic stabilization in hypothetical systems and their realization through chemical synthesis make this a vibrant frontier in scientific advancement.[10−12]

Cyclazines, which possess a peri-fused π-framework with a nitrogen atom occupying the central position, have received special attention compared to simple aromatics.[13,14] Their syntheses generally involve cycloaddition of preformed indolizines or their analogues with suitable alkynes, but other routes employing properly substituted heterocyclic precursors through successive cyclization steps are also known.[15−23] Apart from therapeutic relevance, they show interesting redox and photophysical properties and have potential use in the areas of molecular electronics, solar cells, etc.[18,24,25] An equally interesting group is their carbon analogues in which the central position is occupied by an sp^3 carbon.[26] Topological isomers of such systems, which possess centers carrying either lone pairs of electrons (heteroatom) or a vacant p-orbital in one of the peripheral positions, are also possible but are much less investigated.[27] During our synthetic studies involving indolizinones, we have unraveled a novel reaction pathway that leads to 3′,8a-dihydrocyclopenta[*hi*]indolizin-8a-ol frameworks, which are potential precursors of such systems.[28] The outer rim of atoms in this case is reminiscent of an aza[10]annulene framework that has received both experimental and theoretical interest as the higher aromatic analogue of pyridine (Figure 1).[29]

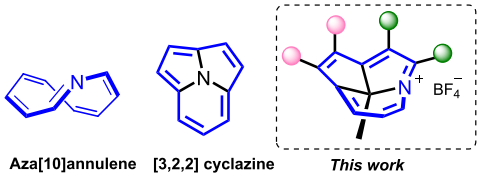

Figure 1. Comparison of the structures of aza[10]annulene and cyclazine with the new analogues reported here.

Though evidence for the formation of a delocalized 10-electron system from these aza-tricyclic precursors was gathered through NMR experiments,[28] their isolation in pure form, crystallographic structure determination, and investigation of chemical characteristics were pending. Our concerted efforts along these lines have given promising results, and this forms the first report on the complete characterization of charged cyclazines with nitrogen on the periphery (Figure 1). Synthesis of aza-tricyclic precursors **3a−g** (Scheme 1) involved [8 + 2] cycloaddition of suitably substituted indolizinones with dimethylacetylene dicarboxylate (DMAD). These reactions also afforded 1,2-dihydropyrrol-3-ones (**2a−g**) as the side products which independently have relevance as anticancer

Received: March 11, 2021
Published: April 27, 2021

© 2021 American Chemical Society

https://doi.org/10.1021/acs.orglett.1c00827
Org. Lett. 2021, 23, 3354−3358

Scheme 1. Synthesis of Charged Cyclazine Analogues 4a−g Possessing an sp^3 Carbon at the Center and Nitrogen Atom on the Periphery

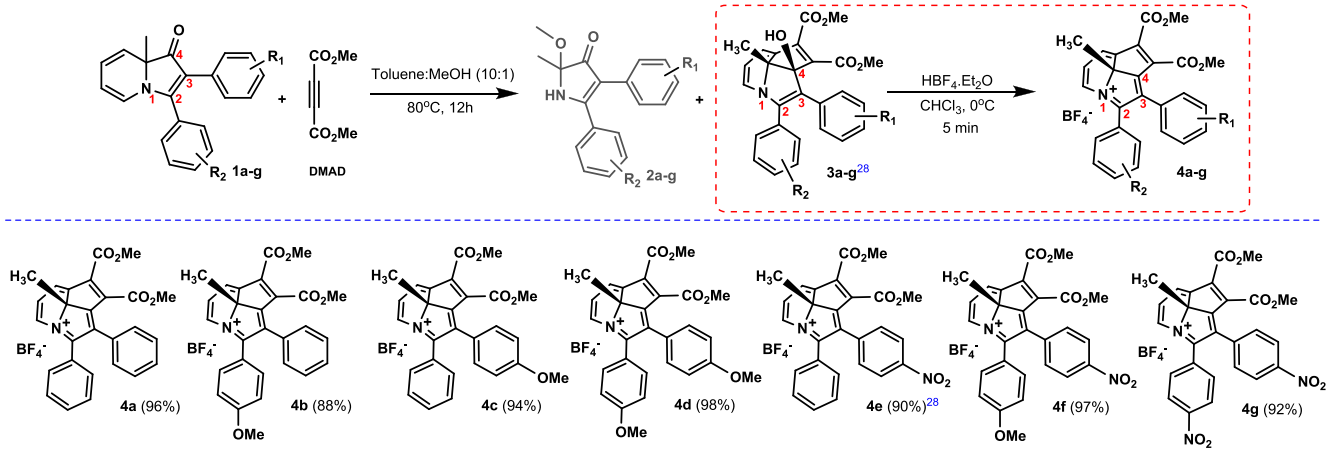

leads.[28,30] Having the peripheral nitrogen and *tert*-hydroxyl group in a 1,4-relationship, dehydration under acidic conditions was expected to give a continuous π-framework with 10 electrons as shown in Scheme 1. After the preparation of **3a** from indolizinone **1a** and DMAD, it was dissolved in chloroform and exposed to $HBF_4{\cdot}Et_2O$ at 0 °C. Complete disappearance of the starting material accompanied by the formation of a highly polar product was observed in just 5 min. Removal of excess $HBF_4{\cdot}Et_2O$ by repeated washing with diethyl ether followed by hexane gave a pure yellow-colored solid (**4a**) in high yield (96%) which was stable for storage under normal laboratory conditions (Supporting Information). HRMS spectrum of this compound had a base peak at m/z = 424.1534, corresponding to the molecular formula $C_{27}H_{22}NO_4$. The same protocol was used to prepare **4b−g** in 88−98% yields from the corresponding precursors (**3b−g**). They were also characterized by a combination of spectro-analytical techniques, details of which are included in the Supporting Information.

In the ^{1}H NMR spectrum, the central CH_3 of **3a** gave a signal at 0.80 ppm whereas in **4a**, the corresponding signal appeared at −0.24 ppm (Figure S37). The olefinic proton signals in **3a** were in the range of 5.90−6.85 ppm, but the corresponding protons in **4a** appeared much farther downfield, between 8.35 and 9.50 ppm. A similar trend was seen in all other compounds in this series, suggestive of a ring current effect (Table S8, Figures S7 and S21). Since the carbon nuclei associated with these protons are also situated in comparable environments, a similar response was anticipated. ^{13}C signals from carbons along the rim shifted downfield as expected. However, instead of an upfield shift, the central CH_3 signal was also found to move downfield, which is atypical (a downfield shift of 16 ppm with respect to the precursor was observed in the case of **4a**; Figure S37). Apart from geometrical aspects, the chemical shift positions are influenced by charge, hybridization states, or electronegativity differences and are important in the present context. During the formation of **4**, the precursor **3** loses the *tert*-hydroxyl group from position-4 (Scheme 1) and also gains a positive charge. These changes could influence the chemical shifts and are likely deshielding in nature. The observed downfield shift in the case of the central $^{13}CH_3$ signal could therefore represent the result of these mutually opposing effects, viz. shielding effect from ring current and deshielding effect from changes in the electronic structure.

The downfield shift of signals from the outer protons and upfield shift of that from the central CH_3, taken together, point toward diamagnetic ring current in **4a−g**, but it is important to note that *aromaticity* is a multidimensional phenomenon and cannot be assessed by magnetic criteria alone.[1,31−36] In light of this, further experimental and theoretical studies by including more structurally related compounds are needed to fully understand the ring current in the present class of molecules.

Since a deeper insight into the structure of **4a−g**, especially the key changes in the core as a result of electron delocalization is possible through X-ray crystallographic analysis, efforts were made to secure diffractable crystals of both starting materials and the products. Gratifyingly, after screening a series of conditions, we succeeded in obtaining crystals of **3d** from methanol and **4d** from $CDCl_3$, and the respective structures are presented in Figure 2. Crystals of **3d**

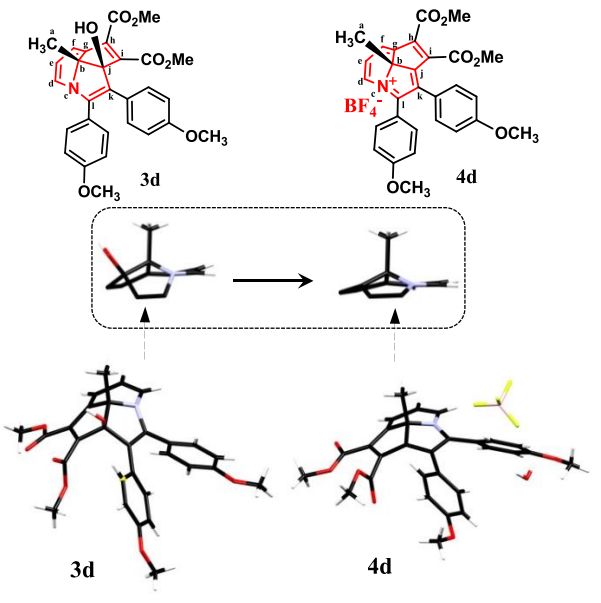

Figure 2. X-ray structures of **3d** and **4d**; side views of the tricyclic core in these compounds are shown separately in the inset. Atomic positions are arbitrarily labeled from a-l; CCDC numbers of **3d** and **4d** are 2043141 and 2043140, respectively.

https://doi.org/10.1021/acs.orglett.1c00827
Org. Lett. 2021, 23, 3354−3358

belonged to the monoclinic system with a $P2_1/c$ space group, whereas those of **4d** were triclinic with a P-1 space group. Details of the crystallographic data are included in Tables S1–S4. The inset of Figure 2 shows the overall change in the tricyclic core as **3d** transforms to **4d**. The central carbon retained sp^3 geometry with minimum compromise from typical bond angles (Table S3), whereas the atoms situated along the outer rim were found to reach a near-planar arrangement to facilitate delocalization of electrons! Hyperconjugative interaction of the central C−CH_3 σ-bond with suitably aligned antibonding orbitals may also be contributing to the overall stability. Notable changes were seen in bond angles and bond lengths around the carbon that carried the *tert*-hydroxyl group. Flattening of the structure is associated with widening of angle $\angle ijk$ from 113.10° (**3d**) to 140.30° (**4d**) as well as $\angle cbg$ from 107.2° (**3d**) to 114.2° (**4d**). A small decrease in bond lengths of C_b−C_j (1.549 to 1.451 Å); N_c−C_l (1.398 to 1.368 Å), C_k−C_j (1.529 to 1.396 Å), C_j−C_i (1.530 to 1.421 Å) and an increase in C_k−C_l bond length (1.354 to 1.425 Å) are also consistent with delocalization effects (Table S4, Figures S1–S3).

Impressive colors of **4a**−**d** in the solid and solution states (Figure 3) and their attractive emission behavior prompted us

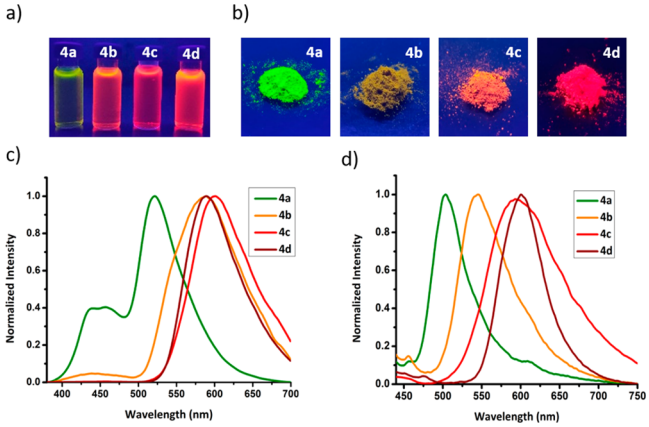

Figure 3. (a) Solutions of **4a**−**d** in DCM when viewed under 352 nm light. (b) Solid samples of **4a**−**d** viewed under 352 nm light. (c) Normalized emission spectra of 3.33×10^{-5} M solutions of **4a**−**d** in DCM. (d) Normalized solid-state emission spectra of **4a**−**d**.

to investigate their photophysical characteristics in a greater detail. Those containing NO_2 group (**4e**, **4g**, and **4f**) were brown gummy solids and were not included in the study.

Absorption spectra of these compounds (**4a**−**d**) were recorded in toluene, dichloromethane (DCM), ethyl acetate, and acetonitrile (Figure S4, Table S5). The spectrum of **4a** in DCM showed three absorption bands at 330, 402, and 490 nm. Similar behavior was observed in toluene and acetonitrile, with slight variation in the wavelengths of absorption. Compounds **4b** and **4c** having an −OMe group at the para-position of the aryl ring at either C-2 or C-3 also exhibited similar absorption behavior (Table S5). The compound **4d** with an −OMe group on both these rings displayed four absorption bands in most of the solvents. The nature of these electronic transitions was analyzed by TD-DFT calculations using the B3LYP/6-31G(d) method, taking **4d** as a representative example (Figure S6 and Table S7). In this compound, the occupied orbitals were found to have their major contribution from the 1,2-diaryl fragment, while the unoccupied orbitals are mainly located on the aza-tricyclic moiety. Therefore, the electronic transitions appear to involve an intramolecular charge transfer from the 1,2-diaryl fragment to the aza-tricyclic core.

The emission spectra of these compounds were subsequently recorded in different solvents (Figure S5). Compound **4a** exhibited dual emission in DCM with λ_{em} at 457 and 520 nm. An identical emission pattern with λ_{em} at 442 and 584 nm was observed in compound **4b**. Their behavior in other solvents such as toluene, ethyl acetate, and acetonitrile were also similar (Table S5). On the contrary, the emission of **4c** having an −OMe group on the C-3 aryl ring displayed a broad emission band in all of the solvents studied; in DCM its λ_{em} was centered around 600 nm. The compound **4d** having −OMe group on C-2 and C-3 aryl rings had an emission at 588 nm in DCM. The emission spectra of these compounds in DCM are shown in Figure 3c, and the data from other solvents are included in Table S5.

The red-shift in emission on introducing −OMe illustrates the tunable photophysical behavior of these cyclazines. The quantum yields of **4a**, **4b**, **4c**, and **4d** in DCM were estimated as 0.3%, 1.24%, 1.82%, and 2.33%, respectively (Table S6). Overall, these observations suggest that the aryl rings at C-2 and C-3 positions exert different electronic effects on the aza-tricyclic core and also show the potential of this unit to act as an efficient acceptor in charge-transfer-mediated photophysical responses.

Conventional flat aromatic molecules exhibit excellent emission in solution, but their solid-state emissions are generally mediocre, which limits their application potential.[37,38] The peripherally conjugated heterocyclic framework discussed here resembles a "Vietnamese hat" with a shallow cone, and could be an ideal framework for developing solid-emissive materials. The structure and lattice arrangement of **4d** presented in Figure 4 shows a number of features which favor this.

The lattice is formed from enantiomers (E1 and E2, Figure 4a) of this molecule arranged in separate rows. The unique geometry of the core along with its substitution pattern prevented them from establishing any significant secondary interaction with one another; the only proximity was seen between C-3 aryl ring of one enantiomer with that of another. They existed in a "parallelly displaced" arrangement, with an offset distance of about 2.7 Å and centroid−centroid distance of 3.17 Å (Figure 4b).[39] At the same time, BF_4^- counterions and cocrystallized water molecules were found to form independent channels and bridge these enantiomers efficiently (Figure S1). On one hand, absence of efficient π-stacking of chromophores can be expected to thwart the quenching process after excitation, and on the other, their interactions involving counterions and the water molecules could decrease rotational possibilities. To know whether these factors would favor good emission in the solid state, a systematic study was carried out. The solid-state emission behavior and spectra of these compounds are shown in Figure 3b,d. The parent molecule **4a** had λ_{em} at 503 nm, whereas the compounds **4b**, **4c**, and **4d** showed emissions at 546, 595, and 601 nm respectively.

The red-shift in emission wavelength with substitution parallels their behavior in solution and provides additional support in favor of the tunable photophysical features of the aza-tricyclic scaffold. The absolute quantum yields of **4a**, **4b**, and **4d** were recorded using an integrating sphere and were found to be 2.85, 4.10, and 11.4, respectively. These values

https://doi.org/10.1021/acs.orglett.1c00827
Org. Lett. 2021, 23, 3354−3358

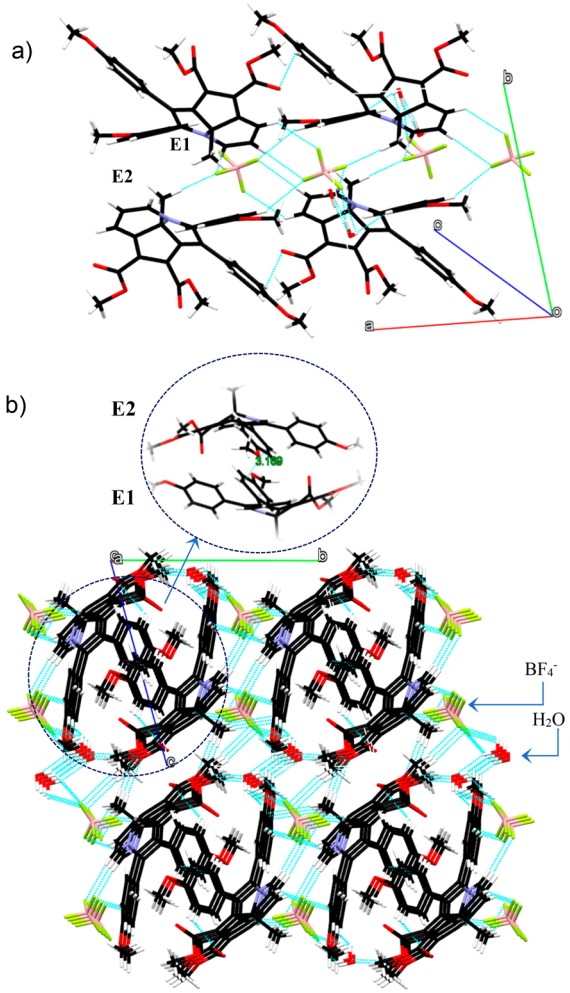

Figure 4. (a) Arrangement of enantiomers of **4a** in the lattice. (b) View of the arrangement of molecules along the *a* axis; BF_4^- counterions and water molecules involved in secondary interactions are also shown.

corresponded to 9.5-, 3.3-, and 5-fold enhancement, respectively, compared to their quantum yields in solution. A compilation of photophysical parameters of **4a**–**4d** is given in Tables S5 and S6.

In summary, this report presents the synthesis and detailed structure analysis of a new group of strained cyclazine analogues, characterized by the presence of a central sp^3 carbon and a nitrogen atom on one of the perepheral positions. Despite having unfavorable angle strain posed by the tetrahedral core, these 10-electron systems showed some NMR characteristics of ring current. They also exhibited prominent charge-transfer-driven photophysical characteristics. The substituents on the C-2 and C-3 aryl rings were able to tune the regions of absorption and emission, leading to an excellent display of colors from green to red, both in solution and solid states.

■ ASSOCIATED CONTENT

Supporting Information

The Supporting Information is available free of charge at https://pubs.acs.org/doi/10.1021/acs.orglett.1c00827.

Experimental procedures and compound characterization data (PDF)

Accession Codes

CCDC 2043140–2043141 contain the supplementary crystallographic data for this paper. These data can be obtained free of charge via www.ccdc.cam.ac.uk/data_request/cif, or by emailing data_request@ccdc.cam.ac.uk, or by contacting The Cambridge Crystallographic Data Centre, 12 Union Road, Cambridge CB2 1EZ, UK; fax: +44 1223 336033.

■ AUTHOR INFORMATION

Corresponding Authors

Muraleedharan Kannoth M. – *Department of Chemistry, Indian Institute of Technology Madras, Chennai 600 036, India*; orcid.org/0000-0001-5711-3557; Email: mkm@iitm.ac.in

Lakshmi Chakkumkumarath – *Department of Chemistry, National Institute of Technology, Calicut, Kerala 673 601, India*; orcid.org/0000-0002-0553-7590; Email: lakshmic@nitc.ac.in

Authors

Jais Kurian – *Department of Chemistry, Indian Institute of Technology Madras, Chennai 600 036, India*

Kanneth S. Shurooque – *Department of Chemistry, National Institute of Technology, Calicut, Kerala 673 601, India*

Venkatachalam Ramkumar – *Department of Chemistry, Indian Institute of Technology Madras, Chennai 600 036, India*

Complete contact information is available at: https://pubs.acs.org/10.1021/acs.orglett.1c00827

Notes

The authors declare no competing financial interest.

■ ACKNOWLEDGMENTS

The financial support of this work by SERB, DST (EMR/2016/003973 and EMR/2016/003306) are gratefully acknowledged. We are also grateful for the infrastructure support by Dept. of Chemistry, IIT Madras, and instrumentation support through its DST-FIST facility. We thank Prof. P. S. Mukherjee (IISc Bangalore) for solid-state emission measurements and Dr. Rini Prakash (IITM) for the help during TD-DFT studies. J.K. thanks IITM and K.S.S. thanks CSIR for their fellowships.

■ DEDICATION

We respectfully dedicate this paper to the memory of (late) Prof. Subramania Ranganathan and (late) Dr. Darshan Ranganathan who remain as the source of inspiration.

■ REFERENCES

(1) Gershoni-Poranne, R.; Stanger, A. Magnetic Criteria of Aromaticity. *Chem. Soc. Rev.* **2015**, *44*, 6597–6615.

(2) Chen, Z.; Wannere, C. S.; Corminboeuf, C.; Puchta, R.; von Ragué Schleyer, P. Nucleus-Independent Chemical Shifts (NICS) as an Aromaticity Criterion. *Chem. Rev.* **2005**, *105*, 3842–3888.

(3) Zhang, X.; Liu, G.; Ganteför, G.; Bowen, K. H.; Alexandrova, A. N. PtZnH5-, A σ-Aromatic Cluster. *J. Phys. Chem. Lett.* **2014**, *5*, 1596–1601.

(4) Spitler, E. L.; Johnson, C. A.; Haley, M. M. Renaissance of Annulene Chemistry. *Chem. Rev.* **2006**, *106*, 5344–5386.

(5) Kaiser, K.; Scriven, L. M.; Schulz, F.; Gawel, P.; Gross, L.; Anderson, H. L. An sp-Hybridized Molecular Carbon Allotrope, Cyclo[18]Carbon. *Science* **2019**, *365*, 1299–1301.

(6) Shin, J. Y.; Kim, K. S.; Yoon, M. C.; Lim, J. M.; Yoon, Z. S.; Osuka, A.; Kim, D. Aromaticity and Photophysical Properties of Various Topology-Controlled Expanded Porphyrins. *Chem. Soc. Rev.* **2010**, *39*, 2751−2767.
(7) Peeks, M. D.; Claridge, T. D. W.; Anderson, H. L. Aromatic and Antiaromatic Ring Currents in a Molecular Nanoring. *Nature* **2017**, *541*, 200−203.
(8) Rickhaus, M.; Jirasek, M.; Tejerina, L.; Gotfredsen, H.; Peeks, M. D.; Haver, R.; Jiang, H. W.; Claridge, T. D. W.; Anderson, H. L. Global Aromaticity at the Nanoscale. *Nat. Chem.* **2020**, *12*, 236−241.
(9) Zubarev, D. Y.; Averkiev, B. B.; Zhai, H. J.; Wang, L. S.; Boldyrev, A. I. Aromaticity and Antiaromaticity in Transition-Metal Systems. *Phys. Chem. Chem. Phys.* **2008**, *10*, 257−267.
(10) Huang, W.; Dulong, F.; Wu, T.; Khan, S. I.; Miller, J. T.; Cantat, T.; Diaconescu, P. L. A Six-Carbon 10π-Electron Aromatic System Supported by Group 3 Metals. *Nat. Commun.* **2013**, *4*, 1448.
(11) Vijay, V.; Madhu, M.; Ramakrishnan, R.; Benny, A.; Hariharan, M. Through-Space Aromatic Character in Excimers. *Chem. Commun.* **2020**, *56* (2), 225−228.
(12) Furukawa, S.; Fujita, M.; Kanatomi, Y.; Minoura, M.; Hatanaka, M.; Morokuma, K.; Ishimura, K.; Saito, M. Double Aromaticity Arising from σ- and π-Rings. *Commun. Chem.* **2018**, *1*, 60.
(13) Matsumoto, K.; Uchida, T.; Yoshida, H.; Kakehi, A. Cycloadditions of Indolizine-3-carbonitriles with Dimethyl Acetylenedicarboxylate: Formation of [2.2.3] Cyclazines and 1:2 Adducts. *J. Chem. Soc., Perkin Trans. 1* **1992**, 2437−2441.
(14) Flitsch, W.; Kramer, U. L. F.; Der Wesqalischen, O.; Vniversitat, W. Cyclazines and Related N-Bridged Annulenes. *Adv. Heterocycl. Chem.* **1978**, *22*, 321−365.
(15) Babaev, E. V.; Simonyan, V. V.; Pasichnichenko, K. Y.; Nosova, V. M.; Kisin, A. V.; Jug, K. Quantum Chemical Analysis and Experimental Study of the Cycloaddition Reaction between Aminoacetylenes and 6-Nitroindolizines. NMR and ab Initio Evidence for the [4 + 2] Adduct Formation. *J. Org. Chem.* **1999**, *64* (25), 9057−9062.
(16) Ghosh, S. K.; Ghosh, D.; Maitra, R.; Kuo, Y. T.; Lee, H. M. Palladium-Catalyzed Oxidative Cyclization for the Synthesis of 2-Alkylimidazo[5,1,2-Cd]Indolizines. *Eur. J. Org. Chem.* **2016**, *2016* (34), 5722−5731.
(17) Aginagalde, M.; Vara, Y.; Arrieta, A.; Zangi, R.; Cebolla, V. L.; Delgado-Camón, A.; Cossío, F. P. Tandem [8 + 2] Cycloaddition-[2 + 6 + 2] Dehydrogenation Reactions Involving Imidazo[1,2- a]Pyridines and Imidazo[1,2- a]Pyrimidines. *J. Org. Chem.* **2010**, *75* (9), 2776−2784.
(18) Lévesque, É.; Bechara, W. S.; Constantineau-Forget, L.; Pelletier, G.; Rachel, N. M.; Pelletier, J. N.; Charette, A. B. General C-H Arylation Strategy for the Synthesis of Tunable Visible Light-Emitting Benzo[a]Imidazo[2,1,5-c,d]Indolizine Fluorophores. *J. Org. Chem.* **2017**, *82* (10), 5046−5067.
(19) Sun, H.; Zhou, H.; Khorev, O.; Jiang, R.; Yu, T.; Wang, X.; Du, Y.; Ma, Y.; Meng, T.; Shen, J. Three-Component, One-Pot Sequential Synthesis of Functionalized Cyclazines: 3 H-1,2a1,3-Triazaacenaphthylenes. *J. Org. Chem.* **2012**, *77* (23), 10745−10751.
(20) Li, P.; Zhang, X.; Fan, X. Synthesis of Naphtho[1′,2′:4,5]-Imidazo[1,2-a]Pyridines and Imidazo[5,1,2-Cd]Indolizines Through Pd-Catalyzed Cycloaromatization of 2-Phenylimidazo[1,2-a]Pyridines with Alkynes. *J. Org. Chem.* **2015**, *80* (15), 7508−7518.
(21) Hu, H.; Li, G.; Hu, W.; Liu, Y.; Wang, X.; Kan, Y.; Ji, M. Synthesis of Pyrrolo[2,1,5-Cd]Indolizines through Dehydrogenative Heck Annelation of Indolizines with Diaryl Acetylenes Using Dioxygen as an Oxidant. *Org. Lett.* **2015**, *17* (5), 1114−1117.
(22) Yu, Y.; Feng, Y.; Chauvin, R.; Ma, S.; Wang, L.; Cui, X. One-Pot Access to Peri-Condensed Heterocycles via Manganese-Catalyzed Cascade C-N and C-C Bond Formation. *Org. Lett.* **2018**, *20* (14), 4209−4212.
(23) Chintawar, C. C.; Mane, M. V.; Tathe, A. G.; Biswas, S.; Patil, N. T. Gold-Catalyzed Cycloisomerization of Pyridine-Bridged 1,8-Diynes: An Expedient Access to Luminescent Cycl[3.2.2]Azines. *Org. Lett.* **2019**, *21* (17), 7109−7113.
(24) Skabeev, A.; Zschieschang, U.; Zagranyarski, Y.; Klauk, H.; Müllen, K.; Li, C. Carbonyl-Functionalized Cyclazines as Colorants and Air-Stable n-Type Semiconductors. *Org. Lett.* **2018**, *20* (5), 1409−1412.
(25) Zheng, W.; Zhao, Y.; Zhuang, W.; Wu, J.; Wang, F.; Li, C.; Zuo, J. Phthalorubines: Fused-Ring Compounds Synthesized from Phthalonitrile. *Angew. Chem.* **2018**, *130* (47), 15610−15615.
(26) Gilchrist, T. L.; Rees, C. W.; Tuddenham, D.; Williams, D. J. 7b-Methy1−7bH-cyclopent[cd]indene-1, 2-dicarboxylic Acid, a New 10 π-Electron Aromatic System; X-Ray Crystal Structure. *J. Chem. Soc., Chem. Commun.* **1980**, 691−692.
(27) Fallah-Bagher-Shaidaei, H.; Farkhonde, R.; Navideh, L. G. Aromaticity of Topological Isomers of Cyclazines and Their [14] to [18] Annulenes. *Comput. Theor. Chem.* **2011**, *963*, 525−532.
(28) Kurian, J.; Kannoth, M. M. Synthesis of New Cyclazines and 4,5-Diaryl-1H-Pyrrol-3(2H)-One Units in Discoipyrroles from Indolizinone-DMAD Cycloadducts. *Org. Biomol. Chem.* **2019**, *17*, 8832−8848.
(29) Bettinger, H. F.; Sulzbach, H. M.; Schleyer, P. V. R.; Schaefer, H. F. Aza[10]Annulene: Next Higher Aromatic Analogue of Pyridine. *J. Org. Chem.* **1999**, *64*, 3278−3280.
(30) Hu, Y.; Potts, M. B.; Colosimo, D.; Herrera-Herrera, M. L.; Legako, A. G.; Yousufuddin, M.; White, M. A.; MacMillan, J. B. Discoipyrroles A-D: Isolation, Structure Determination, and Synthesis of Potent Migration Inhibitors from Bacillus Hunanensis. *J. Am. Chem. Soc.* **2013**, *135*, 13387−13392.
(31) Vernet, R. Du.; Boekelheide, V. Nuclear Magnetic Resonance Spectroscopy. Ring-Current Effects on Carbon-13 Chemical Shifts. *Proc. Natl. Acad. Sci. U. S. A.* **1974**, *71*, 2961−2964.
(32) Mitchell, R. H. Measuring Aromaticity by NMR. *Chem. Rev.* **2001**, *101*, 1301−1315.
(33) Feixas, F.; Matito, E.; Poater, J.; Solà, M. Quantifying Aromaticity with Electron Delocalisation Measures. *Chem. Soc. Rev.* **2015**, *44*, 6434−6451.
(34) Feixas, F.; Matito, E.; Poater, J.; Solà, M. On the Performance of Some Aromaticity Indices: A Critical Assessment Using a Test Set. *J. Comput. Chem.* **2008**, *29*, 1543−1554.
(35) Jug, K.; Köster, A. M. Aromaticity as a Multi-dimensional Phenomenon. *J. Phys. Org. Chem.* **1991**, *4*, 163−169.
(36) Faglioni, F.; Ligabue, A.; Pelloni, S.; Soncini, A.; Viglione, R. G.; Ferraro, M. B.; Zanasi, R.; Lazzeretti, P. Why Downfield Proton Chemical Shifts Are Not Reliable Aromaticity Indicators. *Org. Lett.* **2005**, *7*, 3457−3460.
(37) Bera, M. K.; Pal, P.; Malik, S. Solid-State Emissive Organic Chromophores: Design, Strategy and Building Blocks. *J. Mater. Chem. C* **2020**, *8*, 788−802.
(38) Hong, Y.; Lam, J. W. Y.; Tang, B. Z. Aggregation-Induced Emission. *Chem. Soc. Rev.* **2011**, *40*, 5361−5388.
(39) Ninković, D. B.; Blagojević Filipović, J. P.; Hall, M. B.; Brothers, E. N.; Zarić, S. D. What Is Special about Aromatic-Aromatic Interactions? Significant Attraction at Large Horizontal Displacement. *ACS Cent. Sci.* **2020**, *6*, 420−425.

https://doi.org/10.1021/acs.orglett.1c00827
Org. Lett. 2021, 23, 3354−3358